

Damage identification of isolators in base-isolated torsionally coupled buildings

Jer-Fu Wang¹, Ming-Chih Huang², Chi-Chang Lin^{*3} and Tzu-Kang Lin⁴

¹921 Earthquake Museum of Taiwan, National Museum of Natural Science, Taichung City, Taiwan 413, R.O.C.

²Air Force Institute of Technology, Kaohsiung City, Taiwan 820, R.O.C.

³Department of Civil Engineering, National Chung Hsing University, Taichung City, Taiwan 402, R.O.C.

⁴Department of Civil Engineering, National Chiao Tung University, Hsinchu City, Taiwan 300, R.O.C.

(Received February 29, 2012, Revised October 25, 2012, Accepted November 6, 2012)

Abstract. This paper deals with the damage assessment for isolators of base-isolated building systems considering the torsion-coupling (TC) effect by establishing damage indices. The damage indices can indicate the reduction in lateral stiffness of the isolator story as explicit formulas in terms of modal parameters. In addition, the damage location, expressed in terms of the estimated damage index and eccentricities before and after damage, is also presented. Numerical analysis shows that the proposed algorithms are applicable for general base-isolated multi-story TC buildings. A procedure from the analysis of seismic response to the implementation of damage indices is demonstrated by using a numerical case. A system identification technique is employed to extract modal parameters from seismic responses of a building. Results show that the proposed indices are capable of detecting the occurrence of damage and preliminarily estimating the location of damaged isolator.

Keywords: base isolation; torsion-coupling effect; damage detection; damage locating

1. Introduction

Structural health monitoring (SHM) and structural control have been popular topics for decades because the worldwide increase in long-span bridge and high-rise building under man-made and natural forces brings people more needs in disaster prevention. While the majority of previous studies focused on the damage assessment and vibration control of conventional structures, very few of them take the damage assessment of vibration control devices into consideration.

Base isolation could be the most welcomed strategy among the passive vibration control devices. For a base isolation system subjected to earthquake excitations, the vibration energy is dissipated by the nonlinear hysteretic characteristic of isolator material or interface. Earlier research attempted to apply various mathematical models to simulate the behavior of base isolators where bilinear models received the most interest. Recent researches (Furukawa *et al.* 2005, Huang *et al.* 2009, Oliveto *et al.* 2010, Ventura *et al.* 2003) successfully utilized bilinear models on parameter identifications of base isolation systems. Huang *et al.* (2009) introduced a backbone curve consisting of two constant slopes, representing pre-yielding stiffness and post-yielding

*Corresponding author, Distinguished Professor, E-mail: cclin3@dragon.nchu.edu.tw

stiffness, respectively, and the complex nonlinear problem is replaced with simpler linear problem. They can now apply a system identification scheme for the linear representation of the base isolator system.

Damage assessment based on the change of dynamic characteristics, such as frequency, mode shape, stiffness, and flexibility of buildings, is one approach of interest. Previous studies (Allemang and Brow 1982, Lieven and Ewins 1988, Pandey 1994, Farrar and Jauregui 1998, Elenas and Meskouris 2001, Ndambi *et al.* 2002, Kim *et al.* 2003, Brasiliano *et al.* 2004, Kim and Chun 2004, Wang *et al.* 2007) had demonstrated their attempts to develop damage assessment algorithms based on dynamic parameters, which are generally extracted from vibration measurements of structures. However, these algorithms were generally applied to conventional structures. Extensively, Yoshimoto *et al.* (2005) performed the damage detection of base-isolated buildings by evaluating the stiffness and damping of isolator story based on identified modal parameters. Their study uses a planar building system and the solution is implicitly contained in a least square equation.

To detect damage of a structure by identifying its stiffness information, the system model should be able to reflect the real situation. Conventionally, a regular structural system is assumed in a base isolation problem. However, arrangement of the superstructure or the isolators could be asymmetric. Even though the asymmetry is minimized by strategic placement of isolation devices, single isolator damage could still cause the amplification of system irregularity. Recent studies (Ryan and Chopra 2002, Tena Colunga and Gómez Soberón 2002, Tena Colunga and Zambrana Rojas 2006, Tena Colunga and Escamilla Cruz 2007, Kilar and Koren 2009) show that without concerning the fact of the torsion-coupling (TC) effect due to asymmetry, it is very likely to underestimate the seismic responses of base-isolated buildings. In other words, ignoring the TC effect can lead to inaccurate estimation in dynamic parameters of a system.

The objective of this study is to develop damage detection indices and damage locating indices for isolators of a base isolation system with the TC effect considered. The damage detection index is on the basis that the damage of a base isolator can lead to the reduction in lateral stiffness of the isolator and the change in modal parameters of the system. The idea of damage locating method is based on the fact that damage of partial isolators can cause the change of the center of rigidity (C.R.) of isolator story. Since modal parameters of a structural system can be directly identified by employing system identification techniques based on vibration measurements, characteristic equation is applied to establish the relationship between modal parameter and physical parameter. This study performs numerical analysis on multi-story base-isolated TC buildings to evaluate the accurate range of the proposed methods. A procedure to optimize the mode shape to improve the accuracy of indices is also proposed. Finally, numerical demonstration is conducted to simulate the procedure from seismic response analysis to damage assessment of a base-isolated TC building.

2. Formulation of algorithms

2.1 System model and dynamic equations

A base-isolation system can be modeled as an equivalent linear system, at either the pre-yielding stage or the post-yielding stage (Huang *et al.* 2009). A previous study (Oliveto *et al.* 2010) showed that the first three vibration modes of an asymmetric base-isolation building are primarily of the rigid-body motion of the superstructure when the isolator story experiences large

deformation. Therefore, a rigid superstructure with N_b base isolators, as shown in Fig. 1, is modeled to simulate the dynamic characteristics of a base isolation system. There are three degrees of freedom at the center of mass (C.M.) i.e., two translations relative to ground along x- and y-directions and torsion along θ -direction. Moreover, only shear deformation in the isolator story is considered.

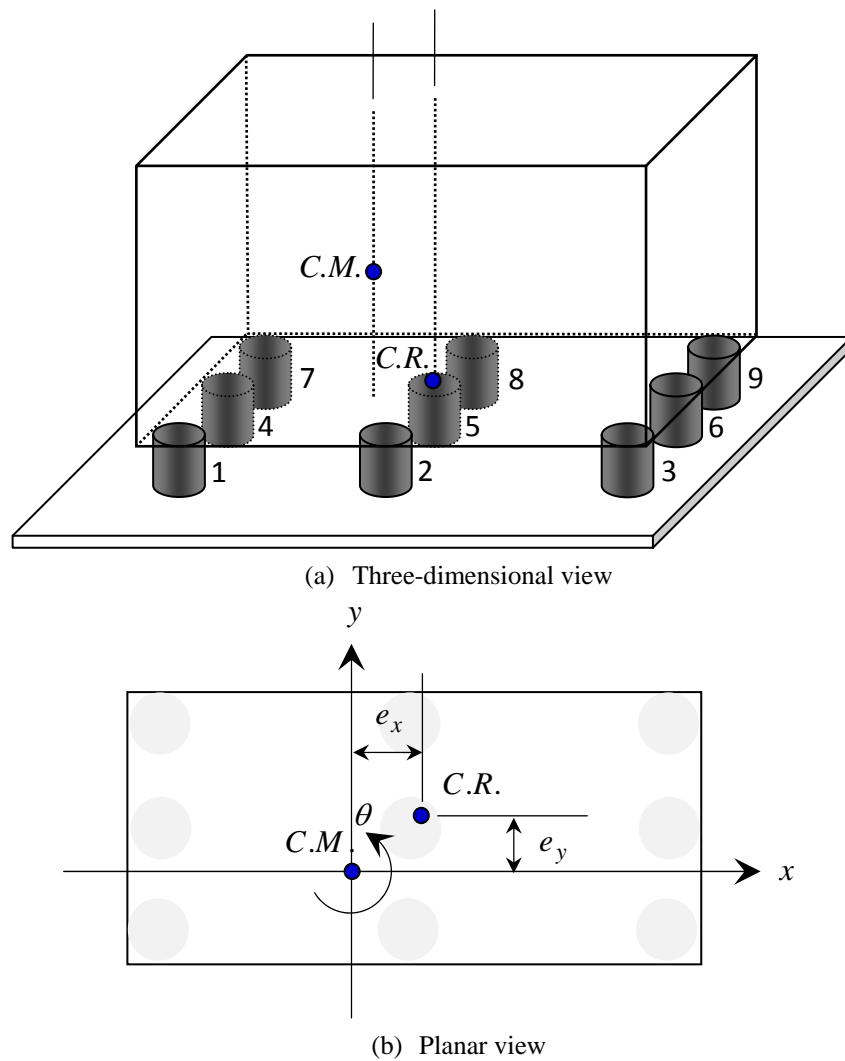


Fig. 1 Rigid-body superstructure base-isolation model

Fig. 2 plots the free-body diagram of the superstructure under bi-directional horizontal ground motions, \ddot{x}_g and \ddot{y}_g , along with the applied forces. The mass and polar moment of inertia of the building are represented as m_p and J_p , respectively. The i th isolator locates at coordinate $(x_i,$

y_i) with origin at the C.M. of the superstructure and has uncoupled stiffnesses, k_{x_i} , k_{y_i} , and k_{θ_i} , along x-, y-, and θ -directions, respectively. All of the isolators form the total uncoupled story stiffnesses, $k_{b_x} (= \sum_i k_{x_i})$, $k_{b_y} (= \sum_i k_{y_i})$, and $k_{b_\theta} (= \sum_i k_{\theta_i})$, along x-, y-, and θ -directions, respectively. Two-way eccentricities between the center of rigidity (C.R.) of the isolators and the C.M. along x- and y-directions are represented as e_x and e_y , which are equal to $(\sum_i k_{y_i} x_i) / \sum_i k_{y_i}$ and $(\sum_i k_{x_i} y_i) / \sum_i k_{x_i}$, respectively. The x-directional displacement, y-directional displacement, and θ -directional torsion at C.M. of the building relative to the ground are denoted as x_p , y_p , and θ_p , respectively.

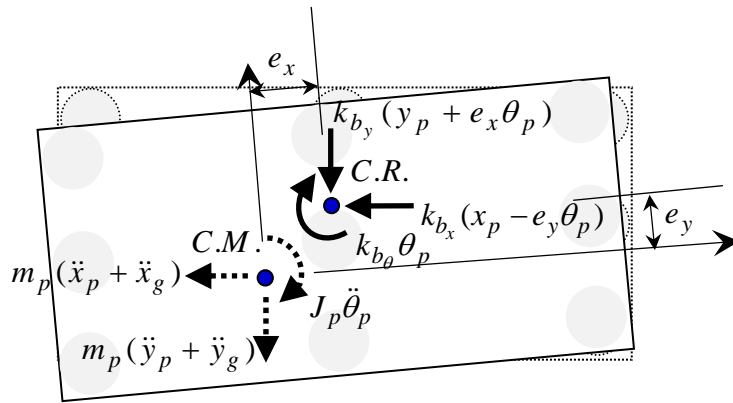


Fig. 2 Free-body diagram and applied forces of base-isolated superstructure

From the force equilibrium in x-, y-, and θ -directions, three equations of motion of the undamped system are given by

$$m_p \ddot{x}_p + k_{b_x} x_p - k_{b_x} e_y \theta_p = -m_p \ddot{x}_g \tag{2.1}$$

$$m_p \ddot{y}_p + k_{b_y} y_p + k_{b_y} e_x \theta_p = -m_p \ddot{y}_g \tag{2.2}$$

$$J_p \ddot{\theta}_p - k_{b_x} e_y x_p + k_{b_y} e_x y_p + (k_{b_x} e_y^2 + k_{b_y} e_x^2 + k_{b_\theta}) \theta_p = 0 \tag{2.3}$$

With damping, the equations of motion of the structural system can be rewritten in matrix form as

$$\mathbf{M}\ddot{\mathbf{U}} + \mathbf{C}\dot{\mathbf{U}} + \mathbf{K}\mathbf{U} = \mathbf{M}\mathbf{r}\ddot{\mathbf{U}}_g \tag{2.4a}$$

where

$$\mathbf{M} = \begin{bmatrix} m_p & 0 & 0 \\ 0 & m_p & 0 \\ 0 & 0 & J_p \end{bmatrix}, \quad \mathbf{K} = \begin{bmatrix} k_{b_x} & 0 & -k_{b_x}e_y \\ 0 & k_{b_y} & k_{b_y}e_x \\ -k_{b_x}e_y & k_{b_y}e_x & k_{b_x}e_y^2 + k_{b_y}e_x^2 + k_{b_\theta} \end{bmatrix} \quad (2.4b, 2.4c)$$

$$\mathbf{U} = \begin{Bmatrix} x_p \\ y_p \\ \theta_p \end{Bmatrix}, \quad \mathbf{r} = \begin{bmatrix} -1 & 0 \\ 0 & -1 \\ 0 & 0 \end{bmatrix}, \quad \ddot{\mathbf{U}}_g = \begin{Bmatrix} \ddot{x}_g \\ \ddot{y}_g \end{Bmatrix} \quad (2.4d-2.4f)$$

where \mathbf{M} , \mathbf{C} , and \mathbf{K} are the 3×3 mass, damping, and stiffness matrices of the system; \mathbf{r} is the 3×2 influence matrix.

Let $\Phi_j = \{\phi_{x_j} \ \phi_{y_j} \ \phi_{\theta_j}\}^T$ be the 3×1 mode-shape vector of the j th mode and ω_j be the j th modal frequency. The relationship between the j th modal parameters and the physical parameters of the system can be established by the characteristic equation as

$$(\mathbf{K} - \omega_j^2 \mathbf{M})\Phi_j = \mathbf{0} \quad (2.5)$$

Substituting Eqs. (2.4b) and (2.4c) into Eq. (2.5), the lateral stiffnesses of the isolator story can be analytically derived as

$$k_{b_x} = \omega_j^2 \frac{m_p}{1 - e_y r_{\phi_x, j}}, \quad k_{b_y} = \omega_j^2 \frac{m_p}{1 + e_x r_{\phi_y, j}} \quad (2.6a, 2.6b)$$

where j is 1, 2, or 3; $r_{\phi_x, j} = \phi_{\theta_j} / \phi_{x_j}$; $r_{\phi_y, j} = \phi_{\theta_j} / \phi_{y_j}$; and e_x and e_y can be expressed in terms of modal parameters as

$$e_x = \frac{\omega_{j_2}^2 - \omega_{j_1}^2}{-\omega_{j_2}^2 r_{\phi_y, j_1} + \omega_{j_1}^2 r_{\phi_y, j_2}}, \quad e_y = \frac{\omega_{j_2}^2 - \omega_{j_1}^2}{\omega_{j_2}^2 r_{\phi_x, j_1} - \omega_{j_1}^2 r_{\phi_x, j_2}} \quad (2.7a, 2.7b)$$

where j_1 and j_2 are two selected modes and $j_1 \neq j_2$. The derivation details from Eq. (2.5) to Eqs. (2.7a) and (2.7b) are shown in the appendix.

2.2 Damage detection index

As mentioned earlier, damage detection indices of the isolator story along x-direction, represented as $R_{k_{b,x}}$, and along y-direction, represented as $R_{k_{b,y}}$, are defined as the reduction in lateral stiffness of the isolator story along x-direction and y-direction, respectively. From Eqs. (2.6) and (2.7), the damage detection indices can be written as

$$R_{k_b,x} = 1 - \frac{k_{b_x}^*}{k_{b_x}} = 1 - \frac{\omega_j^{*2}(1 - e_y r_{\phi_x,j})}{\omega_j^2(1 - e_y^* r_{\phi_x,j}^*)} \quad (2.8a)$$

$$R_{k_b,y} = 1 - \frac{k_{b_y}^*}{k_{b_y}} = 1 - \frac{\omega_j^{*2}(1 + e_x r_{\phi_y,j})}{\omega_j^2(1 + e_x^* r_{\phi_y,j}^*)} \quad (2.8b)$$

where the superscript “*” is used to represent damage state and j is 1, 2, or 3. Observing Eqs. (2.8a) and (2.8b), the proposed damage detection indices require only the modal parameters of the system without necessarily knowing any physical parameters. In this study, for the calculation of $R_{k_b,x}$, the mode with ϕ_{x_j} dominating its mode shape is selected to ensure $r_{\phi_x,j} (= \phi_{\theta_j} / \phi_{x_j})$ is valid. Same consideration is taken for the calculation of $R_{k_b,y}$.

2.3 Damage locating index

Besides a reduction in lateral stiffness, if uneven damage occurs, the new C.R. will move away from the damage components. Therefore, from the position change of C.R., the quadrant (with origin at C.M.) where the damage is located could be determined.

From the definition of eccentricity mentioned previously, the x-directional eccentricities after and before damage can be written as

$$e_x^* = \frac{k_{x_i}^* D_{x_i}^* + (k_{b_x}^* - k_{x_i}^*) D_{x_r}^*}{k_{b_x}^*} \quad (2.9a)$$

$$e_x = \frac{k_{x_i} D_{x_i} + (k_{b_x} - k_{x_i}) D_{x_r}}{k_{b_x}} \quad (2.9b)$$

where k_{x_i} and $k_{x_i}^*$ are the lateral stiffnesses of the damaged isolator in undamaged and damaged states; and k_{b_x} and $k_{b_x}^*$ are the total stiffnesses of the isolator story in undamaged and damaged states, respectively. D_{x_i} and $D_{x_i}^*$ represent the x-coordinate of the center of rigidity of damaged isolators before and after damage; D_{x_r} and $D_{x_r}^*$ indicate the x-coordinate of the center of rigidity of undamaged isolators before and after damage. In fact, $D_{x_r} = D_{x_r}^*$ in any circumstance.

In case of single isolator damage, $D_{x_i}^* = D_{x_i}$ because either D_{x_i} or $D_{x_i}^*$ means the x-coordinate of the location of the damaged isolator. From Eqs. (2.9a) and (2.9b), we have

$$D_{x_i} = \frac{e_x^* k_{b_x}^* (k_{b_x} - k_{x_i}) - e_x k_{b_x} (k_{b_x}^* - k_{x_i}^*)}{k_{x_i}^* k_{b_x} - k_{x_i} k_{b_x}^*} \quad (2.10)$$

Because k_{x_i} is a fraction of k_{b_x} , it is always true that

$$k_{x_i} = R_{x_i} k_{b_x} \quad (2.11)$$

where R_{x_i} is the unknown fraction. In other words, the total stiffness of undamaged isolators, represented as k_{x_r} , can be written as

$$k_{x_r} = (1 - R_{x_i}) k_{b_x} \quad (2.12)$$

In addition, rearranging Eq. (2.8a) yields

$$k_{b_x}^* = (1 - R_{k_{b,x}}) k_{b_x} \quad (2.13)$$

Moreover, $k_{b_x}^*$ is the sum of damaged part, $k_{x_i}^*$, and undamaged part, k_{x_r} , which can be written as

$$k_{b_x}^* = k_{x_i}^* + k_{x_r} = k_{x_i}^* + (1 - R_{x_i}) k_{b_x} \quad (2.14)$$

Equating Eqs. (2.13) and (2.14), the unknown parameter $k_{x_i}^*$ can be expressed as

$$k_{x_i}^* = (R_{x_i} - R_{k_{b,x}}) k_{b_x} \quad (2.15)$$

Substituting Eqs. (2.12) and (2.15), Eq. (2.10) reduces to

$$D_{x_i} = e_x^* - \frac{e_x^* - e_x}{R_{k_{b,x}}} \quad (2.16a)$$

With the same procedure

$$D_{y_i} = e_y^* - \frac{e_y^* - e_y}{R_{k_{b,y}}} \quad (2.16b)$$

The assuming parameter R_{x_i} terminates during the simplification and the x- and y-coordinates of the damage location, D_{x_i} and D_{y_i} , are functions of damage detecting indices and eccentricities before and after damage.

In case of multiple isolator damage, D_{x_i} would be different from $D_{x_i}^*$ if each isolator does not have the same stiffness reduction. Nevertheless, if damage centers on a specific region, D_{x_i} will be close to $D_{x_i}^*$, and Eqs.(2.16a) and (2.16b) are still acceptable.

3. Verification and applicability analysis

In theoretical derivation, a base-isolated system model with rigid superstructure was applied. The applicability of the formulas for damage detection and locating is a concern because a real base-isolated rigid building does not exist. Therefore, a numerical study was performed to evaluate the accuracy of the proposed damage indices with respect to the ratio of fundamental frequency between fixed-based building and isolated rigid building.

3.1 Description of base-isolation system

The system considered is a three-story building with plan size of 20 meters in length (x-direction) and 10 meters in depth (y-direction). Each floor has lumped mass of 144 tons and polar moment of inertia of $6.0 \times 10^3 \text{ t-m}^2$. Two types of stiffness distribution along building height are taken into account: one is uniform distribution; the other is tapered distribution that the first mode shapes of the three uncoupled structures are all linear. The first modal frequency of the fixed-base building is given by ω_{s_1} and damping ratio of each mode is given by 5%. Let k_{p_x} , k_{p_y} , and k_{p_θ} represent the uncoupled lateral stiffness along x-direction, lateral stiffness along y-direction, and torsional stiffness along θ -direction in each story, respectively, and $k_{p_x} : k_{p_y} : k_{p_\theta}$ is 1: 1: 100. The location of the C.R. of each story is at the center of floor plan and eccentricity parameters are $e_x = 2 \text{ m}$ and $e_y = 1 \text{ m}$. There are nine isolators under the building as shown in Fig. 1. The stiffness of each isolator is set so that the ratio of torsional frequency to lateral frequency (denoted as ω_b) of the isolated rigid system is equal to 4.0. Table 1 presents the analytical expression in representing the story stiffness of the superstructure, the floor mass (m_f), and the stiffness of single isolator.

3.2 Setup of damage scenarios

(i) Case 1 (Single Isolator Damage): The No.2 isolator of the 9-bearing isolation system loses 15% of stiffness in both lateral and torsional directions. Table 2 lists the related damage information.

(ii) Case 2 (Three Isolators Damage): Three isolators have following stiffness losses: 20% in No.1 along the x- and y-directions, 10% in No.2 along the x-direction, and 10% in No.4 along the y-direction. Related information is presented in Table 2. In this case, the exact damage location is within the region enclosed by No. 1, No. 2, and No. 4 isolators.

To investigate the influence of the flexibility of superstructure on the proposed damage detection and locating indices, the values of ω_{s_1} / ω_b considered range from 1 to 30 in both cases.

Table 1 Story stiffnesses of two different distribution types (m_f : floor mass; $a_0 = m_f \omega_{s_1}^2$)

Dir.	Stiffness Distribution Type	
	Type 1	Type 2
x and y	<p> $k_{x_3}, k_{y_3} = 5.049a_0$ $k_{x_2}, k_{y_2} = 5.049a_0$ $k_{x_1}, k_{y_1} = 5.049a_0$ $k_{b_{x_i}}, k_{b_{y_i}} = 632 \text{ t/m}$ </p>	<p> $k_{x_3}, k_{y_3} = 3a_0$ $k_{x_2}, k_{y_2} = 5a_0$ $k_{x_1}, k_{y_1} = 6a_0$ $k_{b_{x_i}}, k_{b_{y_i}} = 632 \text{ t/m}$ </p>
	θ	<p> $k_{\theta_3} = 504.9a_0$ $k_{\theta_2} = 504.9a_0$ $k_{\theta_1} = 504.9a_0$ $k_{b_{\theta_i}} = 4.21 \times 10^5 \text{ t-m}$ </p>

3.3 Selection of mode-shape set

Because the superstructure is flexible, the entire isolation system is no longer an equivalent one-story TC system. To establish the mass and stiffness matrices of this system, the multi-story TC building model developed by Ueng *et al.* (2000) is employed. Then, by solving the eigenproblem, modal frequencies and mode shapes of the isolation system can be obtained. Notice that the mode shape vector of a specific mode can be divided into four sets. Each set has three components which correspond to the x-translation, y-translation, and θ -torsion at the C.M. of a floor (Base, 1F, 2F, or RF). Because only one mode shape set is needed for the calculation of damage indices, different sets are respectively selected to compare the results.

Table 2 Exact damage information of simulated damage scenarios

Case Label	Case 1		Case 2	
Damaged Bearing(s) and Scenarios	No.2 – 15 % stiffness loss in both dirs.		No.1 – 20 % stiffness loss in both dirs. No.2 – 10 % stiffness loss in x dir. No.4 – 10 % stiffness loss in y dir.	
Direction	x	y	x	y
Stiffness Reduction of Isolation Story ($R_{b_x} R_{b_y}$)	0.0167	0.0167	0.033	0.033
Coordinate of Damage Location ($D_{x_i} D_{y_i}$) (m)	2	-4	-4.7	-2.35
Eccentricity Change ($e_x^* - e_x e_y^* - e_y$) (m)	0	0.0847	0.23	0.115

3.4 Discussion of results

(i) Case 1: The calculated damage detection indices, eccentricity changes, and damage locating indices for Type 1 and Type 2 stiffness-distribution cases versus ω_{s_1} / ω_b are presented in Fig. 3 and Fig. 4, respectively. There are four curves in each plot. Each curve corresponds to different selection of mode shape set. The shadow region marks the range of $\pm 10\%$ estimated error from the exact solution for each corresponding ω_{s_1} / ω_b . It is shown that when ω_{s_1} / ω_b increases, the results are asymptotically close to the exact solutions and are less related to the selection of mode shape set, which fits the behavior of a base-isolated rigid-body superstructure.

On the other hand, the estimated error is amplified when the superstructure is flexible. This is due to the fact that the modal frequency (ω_j) and the mode shape ratios ($r_{\phi_x, j}$ and $r_{\phi_y, j}$) are different from those of the rigid superstructure system. It is obvious that $R_{k_b, x}$ has little connection with the adopted mode shape set. This is because that the second mode, having mode shape with $\phi_{\theta, 2} \approx 0$ at each floor, is used to calculate $R_{k_b, x}$. In this condition, Eq. (2.8a) reduces to $R_{k_b, x} = 1 - (\omega_2^* / \omega_2)$, that is not related to the selection of mode-shape set. The trend of $R_{k_b, x}$ also implies that the damage in isolated story could be “diluted” due to the soft superstructure. The estimated error of $R_{k_b, y}$ is more dependent on the adopted mode shape set because the first mode shape is used and all its mode-shape components are not zero. The absolute error can exceed 10% when the mode shape set corresponding to base is used and $\omega_{s_1} / \omega_b < 6$. It also seen that selecting

mode-shape set of upper floors could increase the ω_{s1} / ω_b range where the accuracy of damage detection index is acceptable.

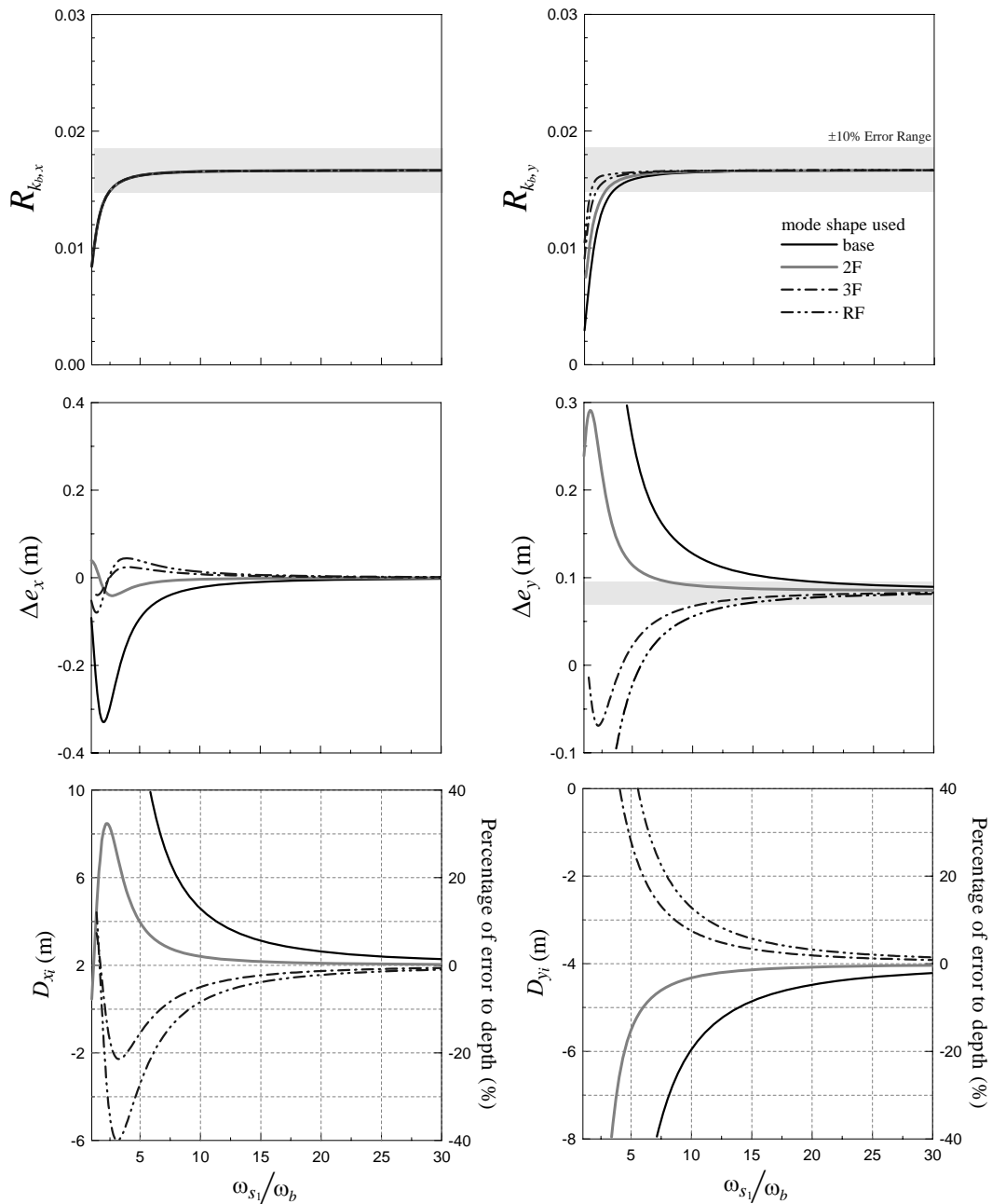


Fig. 3 Damage assessment of three-story base-isolated TC building with Type 1 stiffness distribution with various ω_{s1} / ω_b under Case 1 damage scenario

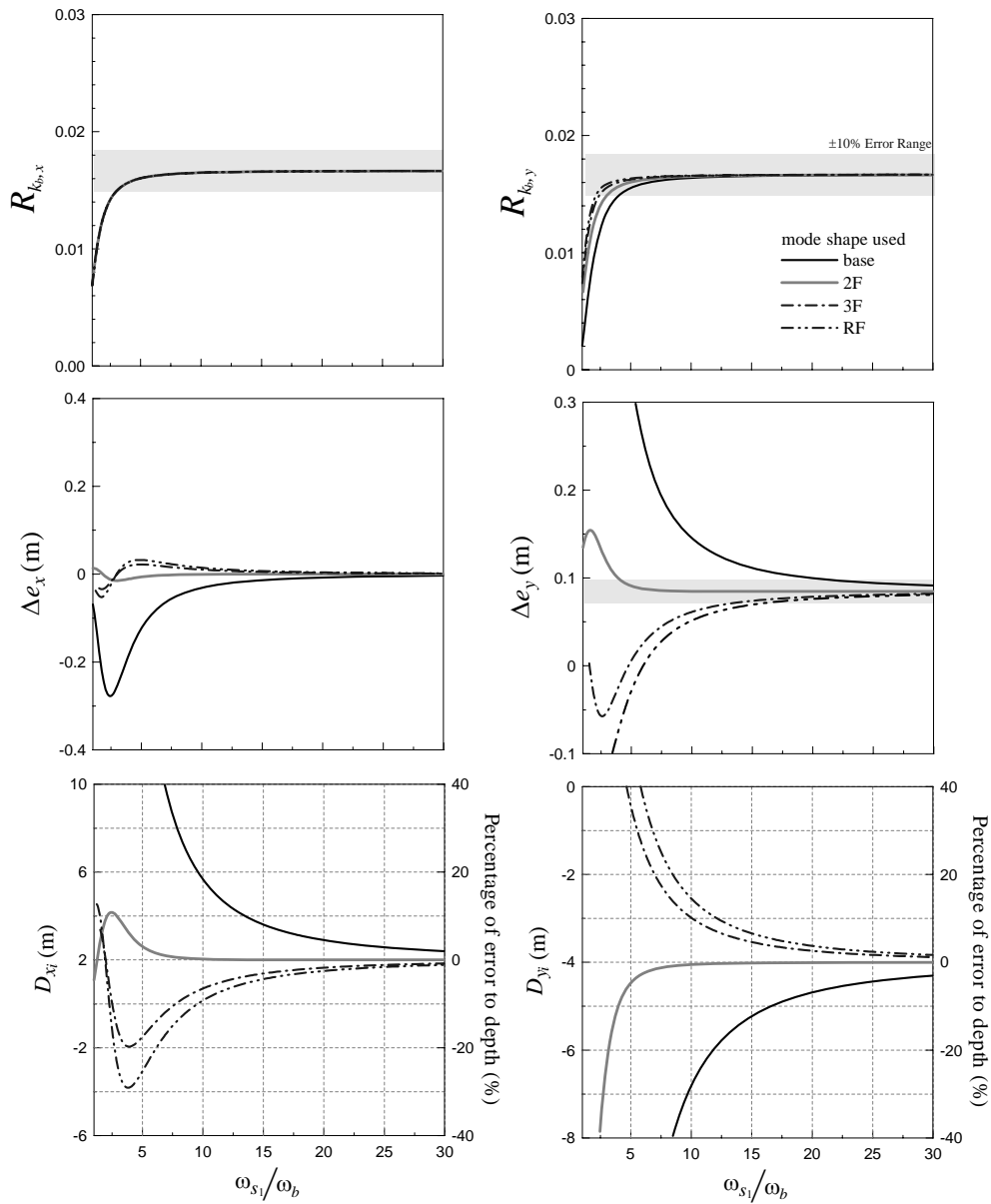


Fig. 4 Damage assessment of three-story base-isolated TC building with Type 2 stiffness distribution with various ω_{s1}/ω_b under Case 1 damage scenario

The estimated damage locating indices (D_{x_i} and D_{y_i}) are more sensitive to the change in flexibility of the superstructure than $R_{k_{b,x}}$ and $R_{k_{b,y}}$. This is due to the high sensitivity of the estimated eccentricity changes, Δe_x and Δe_y , which are used for computing the damage locating

indices. The ratio of estimated error of D_{x_i} to the floor width and estimated error of D_{y_i} to the floor depth can exceed 10 % even when ω_{s_1} / ω_b is as high as 15. The difference between the estimated results of Type 1 and Type 2 stiffness distributions is insignificant but recognizable. This is because that $r_{\phi_{x,j}}$ and $r_{\phi_{y,j}}$ of these two types are different at the same level.

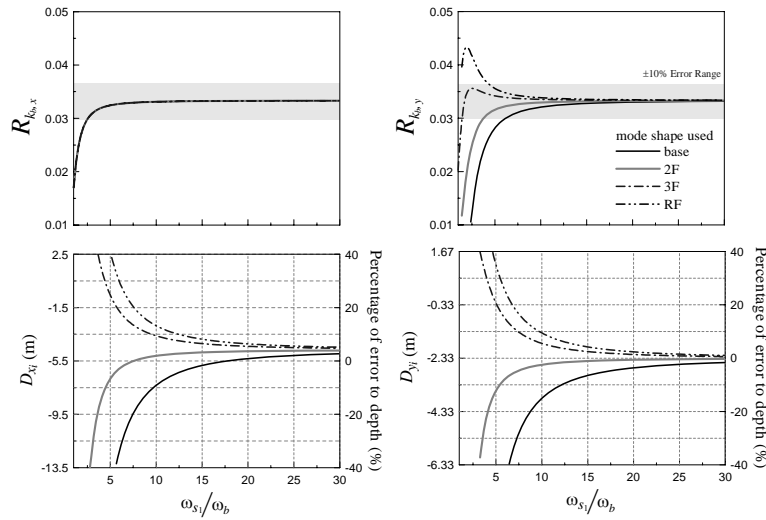


Fig. 5 Damage assessment of three-story base-isolated TC building with Type 1 stiffness distribution with various ω_{s_1} / ω_b under Case 2 damage scenario

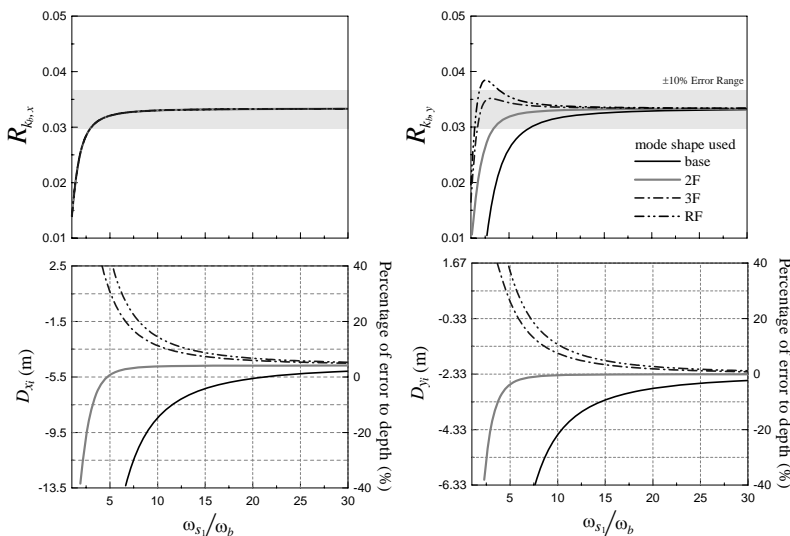


Fig. 6 Damage assessment of three-story base-isolated TC building with Type 2 stiffness distribution with various ω_{s_1} / ω_b under Case 2 damage scenario

(ii) Case 2: The estimated results for Case 2 damage scenario are shown in Figs. 5 and 6. It shows that the proposed method can approximately detect the corresponding stiffness reduction of the isolator story based on the modal parameter information when ω_{s_1} / ω_b is large enough. The influence of flexible superstructure on the accuracy of estimated results is similar to those in Case 1 damage scenario. Both Type 1 and Type 2 cases show that using the mode shape set corresponding to 2F obtains higher accuracy. This implies that if the mode shape set is optimized the estimated error can be minimized when the isolated superstructure is not rigid.

3.5 Optimal mode shape combination factor

Because accelerometers are commonly instrumented at the base and roof of a superstructure in practice, the optimal mode shape set is defined as the linear combination of mode shape sets corresponding to base and roof, and written as

$$\begin{Bmatrix} \phi_{x_j, \text{opt}} \\ \phi_{y_j, \text{opt}} \\ \phi_{\theta_j, \text{opt}} \end{Bmatrix} = \alpha \begin{Bmatrix} \phi_{x_j, \text{roof}} \\ \phi_{y_j, \text{roof}} \\ \phi_{\theta_j, \text{roof}} \end{Bmatrix} + (1 - \alpha) \begin{Bmatrix} \phi_{x_j, \text{base}} \\ \phi_{y_j, \text{base}} \\ \phi_{\theta_j, \text{base}} \end{Bmatrix} \quad (3.1)$$

where α is the combination factor and is a constant between 0 and 1. Then, the optimization problem is to find the optimal combination factor, $(\alpha)_{\text{opt}}$, for the minimization of f_{err} which is defined as

$$\begin{aligned} f_{\text{err}} = & \beta \left[\frac{(R_{k_b, x})_{\text{estimated}} - (R_{k_b, x})_{\text{exact}}}{(R_{k_b, x})_{\text{exact}}} + \frac{(R_{k_b, y})_{\text{estimated}} - (R_{k_b, y})_{\text{exact}}}{(R_{k_b, y})_{\text{exact}}} \right] \\ & + (1 - \beta) \left[\frac{(D_{x_i})_{\text{estimated}} - (D_{x_i})_{\text{exact}}}{(D_{x_i})_{\text{exact}}} + \frac{(D_{y_i})_{\text{estimated}} - (D_{y_i})_{\text{exact}}}{(D_{y_i})_{\text{exact}}} \right] \end{aligned} \quad (3.2)$$

where β is the weighting factor between 0 and 1 to evaluate the importance between the error of damage detection index and the error of damage locating index. In this study, β was set to be 0.5 to balance the errors from each.

By applying searching technique for optimization, the optimal combination factors, $(\alpha)_{\text{opt}}$, obtained versus ω_{s_1} / ω_b for Case 1 and Case 2 are illustrated in Figs. 7(a) and (b). These figures show that the values of $(\alpha)_{\text{opt}}$ change little when ω_{s_1} / ω_b ranges from 4 to 30. Moreover, $(\alpha)_{\text{opt}}$ for the case of Type 2 is always larger than that for the case of Type 1. For the building of Type 1 stiffness distribution, both Case 1 and Case 2 damage scenarios result in similar $(\alpha)_{\text{opt}}$ with a mean value of 0.59 when considering two digits of decimal. For the building of Type 2 stiffness distribution, a mean value of 0.65 could approximately represent $(\alpha)_{\text{opt}}$.

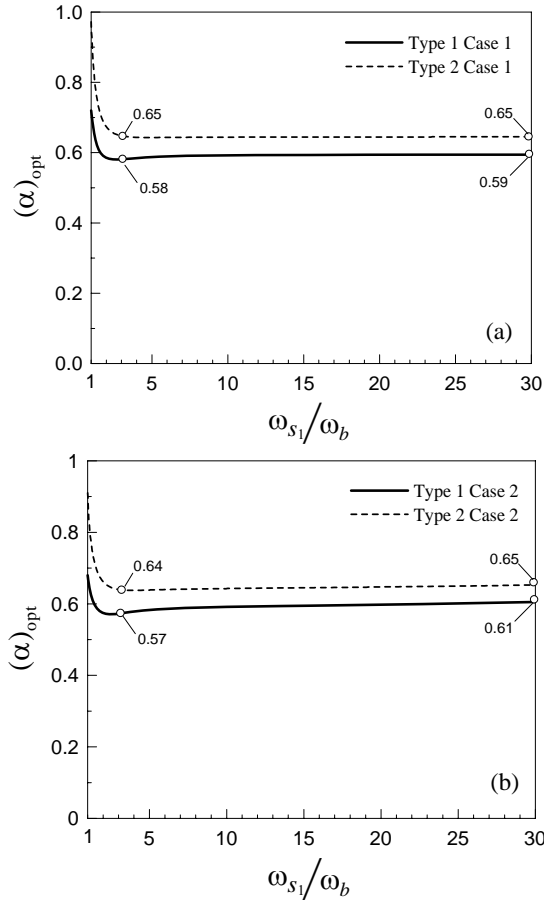


Fig. 7 Optimal mode shape selection factor, α , for Type 1 and Type 2 three-story building isolated system with various ω_{s_1} / ω_b under (a) Case 1 (b) Case 2 damage scenarios

Figs. 8(a) and (b) present the estimated $R_{k_b,x}$ and $R_{k_b,y}$ based on the $(\alpha)_{opt}$ obtained under corresponding ω_{s_1} / ω_b . More acceptable results than the previous analyses are observed. Fig. 8(c) directly maps the estimated damage location on the building plan for ω_{s_1} / ω_b ranging from 2 to 30. It shows that most of the points are near the exact damage locations, which are located at coordinate (2 m, -4 m) for Case 1 and at coordinate (-4.7 m, -2.35 m) for Case 2. Now, let $\alpha = 0.59$ for the building of Type 1 and $\alpha = 0.65$ for the building of Type 2 regardless of the damage scenarios and ω_{s_1} / ω_b . Performing the same analyses, the results are presented in Fig. 9. It shows that $R_{k_b,x}$ and $R_{k_b,y}$ still agree with those in Fig. 8, except when $\omega_{s_1} / \omega_b < 2.5$. From Fig. 9(c), the error in the estimated damage location appears more detectable compared with Fig. 8(c). Nevertheless, the estimated results seem to be acceptable when $\omega_{s_1} / \omega_b > 3.5$.

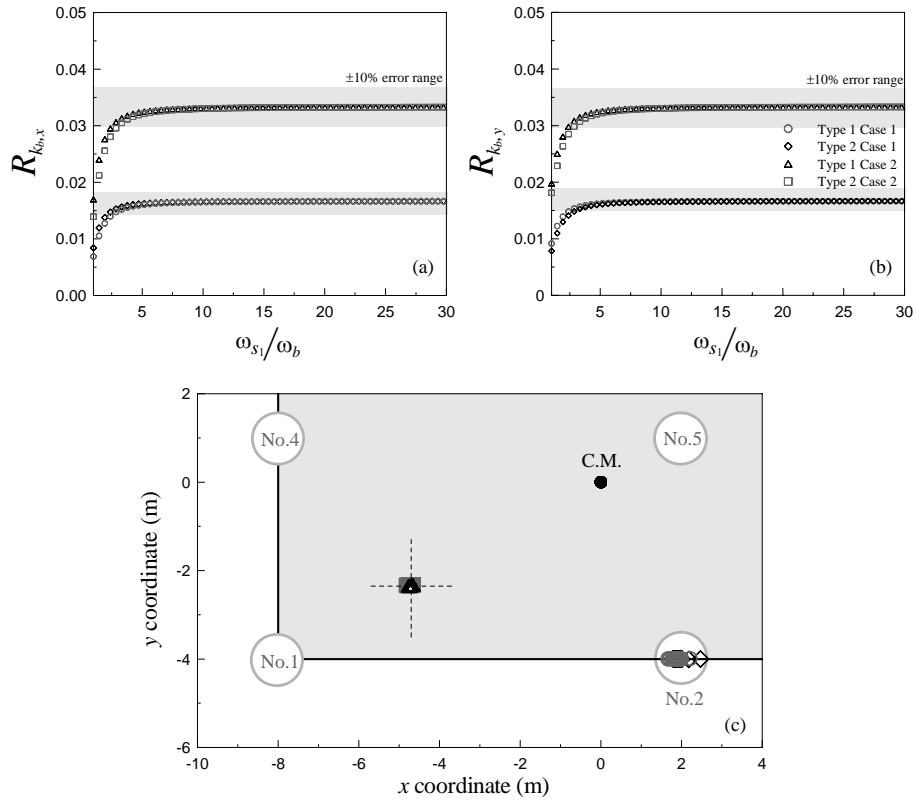


Fig. 8 Damage assessment of three-story base-isolated TC building based on optimal α with various ω_{s_1} / ω_b : (a) Damage index in x direction, (b) Damage index in y direction and (c) Mapping of estimated damage location for ω_{s_1} / ω_b ranging from 2 to 30 (No.1, No.2, No.4, and No.5 represent isolator labels)

4. Numerical demonstration

The numerical demonstration of proposed damage assessment procedure consisted of generation of seismic response of a base-isolated building, identification of dynamic parameters of the system, and computation of the damage algorithms.

4.1 Description of isolated building

The system considered is a four-story base-isolated TC building. The plan size of building floor is 80 m in length (x-direction) and 60 m in depth (y-direction). The floor mass is 2,880 tons and the polar moment of inertia of floor is $9.6 \times 10^6 \text{ t}\cdot\text{m}^2$. The superstructure has Type 2 stiffness distribution along height. The uncoupled natural frequency of the fixed-base superstructure along y-direction is 2.3 Hz. In addition, $k_{p_x} : k_{p_y} : k_{p_\theta} = 1.5 : 1 : 100$. Assume that the C.R. of each

story is at the vertical line passing through the center of each floor with $e_x = -8\text{m}$ and $e_y = -6\text{ m}$. Twenty isolators are installed beneath the building base.. The lateral stiffness of each isolator is set so that the isolated rigid-body system has uncoupled lateral frequency of 0.5 Hz and torsional frequency of 2 Hz. Table 3 presents the stiffness and mass information of this base-isolated building. For simplicity, Rayleigh damping is assumed with damping ratio of 10% for the first three modes, and 5% for the rest higher modes.

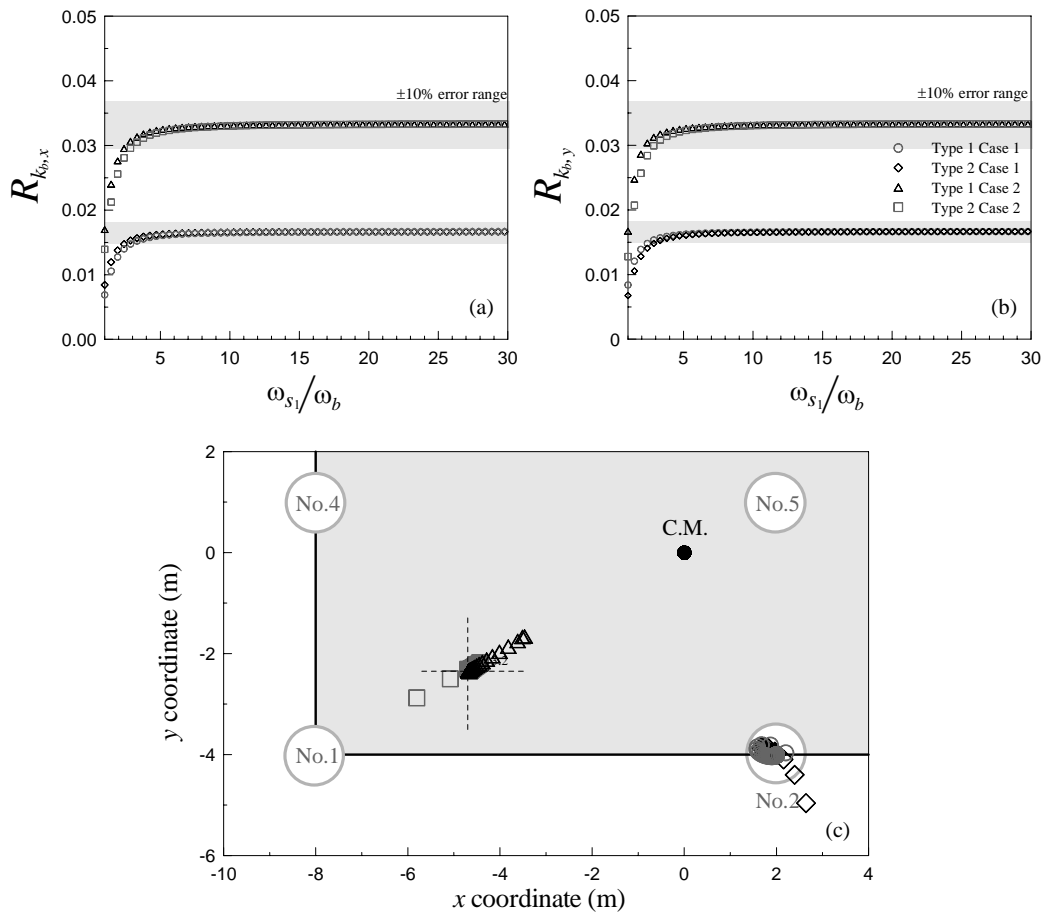


Fig. 9 Damage assessment of three-story base-isolated TC building with $\alpha = 0.59$ for Type 1 and $\alpha = 0.65$ for Type 2 with various ω_{s_1} / ω_b : (a) Damage index in x direction, (b) Damage index in y direction and (c) Mapping of estimated damage location for ω_{s_1} / ω_b ranging from 2 to 30 (No.1, No.2, No.4, and No.5 represent isolator labels; digital numbers label the corresponding ω_{s_1} / ω_b of points)

Table 3 Properties of a base-isolated four-story building

Direction	Mass (t)		Stiffness (t/m)	
x	RF	2880	4S	3.61×10^6
	4F		3S	6.32×10^6
	3F		2S	8.12×10^6
	2F		1S	9.02×10^6
	1F (Base)		Single isolator	7.11×10^4
y	RF	2880	4S	2.41×10^6
	4F		3S	4.21×10^6
	3F		2S	5.41×10^6
	2F		1S	6.01×10^6
	1F (Base)		Single isolator	7.11×10^4
θ	RF	2880	4S	2.41×10^8
	4F		3S	4.21×10^8
	3F		2S	5.41×10^8
	2F		1S	6.01×10^8
	1F (Base)		Single isolator	9.47×10^7

4.2 Damage scenario

Different degrees (2% ~ 10%) of damage at No. 1, No. 2, No. 3, No. 6, No. 7, and No.11 isolators are given as shown in Table 4. Notice that each isolator has the same degree of stiffness loss in both lateral and torsional directions. Under this damage scenario, the stiffness reduction in the isolator story is 1.3%. The exact coordinate of damage location is (-39.5 m, -27.5 m), indicated as a star sign labeled with symbol D_{exact} in Table 4. The system input excitations used for the pre-damage and post-damage events are the N90E component and N00E component of two real earthquake ground accelerations recorded on July 26, 2009 and January 4, 2010, in Hualien, Taiwan.

All input excitations are raw measurement data which contain noise. For the pre-damage event, the standard deviations (STDs) of ambient noise in two components are 0.0157gal and 0.0257gal, respectively. The corresponding STD ratios of the noise to the entire signal are 2.2% and 2.8%. For the post-damage event, the STDs of ambient noise in two components are 0.0332gal and

Table 5 Identified first three modal parameters of four-story building

Events	Pre-damage event	Post-damage event
Modal frequency (Hz)	$\begin{Bmatrix} 0.477 \\ 0.494 \\ 0.767 \end{Bmatrix}$	$\begin{Bmatrix} 0.476 \\ 0.491 \\ 0.764 \end{Bmatrix}$
Mode shape	$\begin{Bmatrix} -0.540 & 0.958 & -0.754 \\ 0.865 & 0.630 & 1.000 \\ 0.0012 & -0.0001 & -0.010 \\ -0.624 & 1.000 & 0.070 \\ 1.000 & 0.664 & -0.093 \\ 0.012 & -0.0007 & -0.149 \end{Bmatrix}$	$\begin{Bmatrix} -0.512 & 0.959 & -0.755 \\ 0.874 & 0.663 & 1.000 \\ 0.0014 & -0.0002 & -0.010 \\ -0.589 & 1.000 & 0.071 \\ 1.000 & 0.700 & -0.094 \\ 0.011 & -0.0003 & -0.156 \end{Bmatrix}$

4.3 Seismic response and system identification

The entire system is equivalent to a five-story TC building system with different properties at the isolator story in pre-damage and post-damage states. The first step is to construct the 15×15 mass, damping, and stiffness matrices of the system corresponding to two different states. Applying the function 'lsim' in Control System Toolbox of mathematics software, MATLAB, the floor accelerations along x -, y -, and θ -directions of the isolated system building subjected to the bi-directional ground motion are obtained. Next, assume that the dynamic parameters of the isolation system are unknown and the prior known information of the system is the floor acceleration responses and the ground inputs. To obtain the modal parameters of the system in damaged and undamaged states, a system identification technique named System Realization using Information Matrix (SRIM) (Juang 1997, Lin *et al.* 2005), is employed. Here, the system inputs considered are the bi-directional ground accelerations, and the system outputs are the lateral and torsional floor accelerations. Followed by using an extraction procedure (Lin *et al.* 2005), the modal frequencies and mode shapes of the first three modes of the isolated system are obtained and addressed in Table 5. Note that the output floor acceleration responses are generated through numerical calculation. To simulate noise contamination, a white noise with STD of 0.0303gal is added to each simulated response. The noise level is based on the observation of measured input signals.

4.4 Damage detection and locating

With the identified modal parameters, the eccentricities in undamaged and damaged states are calculated by Eqs. (2.8a) and (2.8b) with $j_1 = 2$ and $j_2 = 3$. Since the superstructure has Type 2 stiffness distribution, the weighting factor $\alpha = 0.65$ is given. The damage detection indices, $R_{k_b, x}$ and $R_{k_b, y}$, and the damage locating indices, D_{x_i} and D_{y_i} , are calculated according to

Eqs. (2.9a) and (2.9b), and Eqs. (2.16a) and (2.16b), respectively. Table 4 lists all of the results along with the exact solutions. It shows that the estimated $R_{k_b,x}$ and $R_{k_b,y}$ are larger than 0, which indicates the occurrence of damage in the isolator story. The average estimation error of the damage detection indices is acceptable with the consideration of measurement noise. The errors of estimated damage locating indices seem to be a little significant. Nevertheless, from the drawing in Table 4, the estimated damage location, labeled as a solid star, still provides useful information for further damage investigation.

5. Conclusions

In this study, algorithms for damage detection and locating for isolators of a base-isolated building with the assumption of rigid superstructure are proposed. The idea is based on the fact that isolator damage may cause reduction of lateral stiffness in the isolator. According to the theoretical developments and numerical verifications, the following conclusions can be drawn:

(i) Damage detection indices and damage locating indices are presented with simple expressions in terms of modal frequency and mode shape of two selected vibration modes of base-isolated systems. These indices are useful for practical application since the system identification techniques to extract modal parameters from vibration measurements are available.

(ii) A base-isolated TC building with non-rigid superstructure is used to examine the applicability of the proposed methods. The numerical verification results show that the damage detection index is more reliable than the damage locating index because the latter is sensitive to the identification accuracy of the eccentricity. Using the mode shape set corresponding to the three degrees of freedom of different floors for the calculation of the proposed formulas, variant accuracies are obtained. Generally, mode shape set corresponding to base or roof induces unpredictable results when the natural frequency of the fixed-base building is close to that of isolator story. Mode shape set near middle story could give better accuracy.

(iii) An optimization process is performed to obtain an optimal weighting factor used to combine the mode shape set of base and roof. The results show that the accuracies of damage detection index and damage locating index are improved with the optimal weighting factor.

(iv) The numerical demonstration illustrates the procedure to employ the proposed damage assessment of a multi-story base-isolated TC building. With the modal parameters extracted from system measurements using a system identification technique, the proposed damage indices give acceptable results in detecting and locating damaged isolators.

Acknowledgements

This work was supported by the National Science Council of the Republic of China under Grant NSC 99-2625-M-344-001. This support is greatly appreciated.

References

Allemang, R.J. and Brown, D.L. (1982), "A correlation coefficient for modal vector analysis", *Proceedings of the International Modal Analysis Conference & Exhibit*, 110-116.

- Brasiliano, A., Doz, G.N. and Brito, J.L.V. (2004), "Damage identification in continuous beams and frame structures using the residual error method in the movement equation", *Nucl. Eng. Des.*, **227**(1), 1-17.
- Elenas, A. and Meskouris, K. (2001), "Correlation study between seismic acceleration parameters and damage indices of structures", *Eng. Struct.*, **23**(6), 698-704.
- Farrar, C.R. and Jauregui, D.A. (1998), "Comparative study of damage identification algorithms applied to a bridge", *Smart Materials and Structures*, **7**(5), 704-731.
- Furukawa, T., Ito, M., Izawa, K. and Noori, M.N. (2005), "System identification of base-isolated building using seismic response data", *J. Eng. Mech. - ASCE*, **131**(3), 268-275.
- Huang, M.C., Wang, Y.P., Chang, J.R. and Chen, Y.H. (2009), "Physical-parameter identification of base-isolated buildings using backbone curves", *J. Struct. Eng. - ASCE*, **135**(9), 1107-1114.
- Juang, J.N. (1997), "System realization using information matrix", *J. Guid. Control Dynam.*, **21**(3), 492-500.
- Kilar, V. and Koren, D. (2009), "Seismic behaviour of asymmetric base isolated structures with various distributions of isolators", *Eng. Struct.*, **31**(4), 910-921.
- Kim, J.T., Ryu, Y.S., Cho, H.M. and Stubbs, N. (2003), "Damage identification in beam-type structures: frequency-based method vs. mode-shape-based method", *Eng. Struct.*, **25**(1), 57-67.
- Kim, H.S. and Chun, Y.S. (2004), "Structural damage assessment of building structures using dynamic experimental data", *Struct. Des. Tall Spec.*, **13**(1), 1-8.
- Lieven, N.A.J. and Ewins, D.J. (1988), "Spatial correlation of mode shapes, the coordinate modal assurance criterion (COMAC)", *Proceedings of the Sixth International Modal Analysis Conference*, 690-695.
- Lin, C. C., Wang, C. E., Wu, H. W. and Wang, J. F. (2005), "On-line building damage assessment based on earthquake records", *Smart Mater. Struct.*, **14**(3), S137-S153.
- Ndambi, J.M., Vantomme, J. and Harri, K. (2002), "Damage assessment in reinforced concrete beams using eigenfrequencies and mode shapes derivatives", *Eng. Struct.*, **24**(4), 501-515.
- Oliveto, N.D., Scalia, G. and Oliveto, G. (2010), "Time domain identification of hybrid base isolation systems using free vibration tests", *Earthq. Eng. Struct. D.*, **39**(9), 1015-1038.
- Pandey, A.K., Biswas M. and Samman, M.M. (1991), "Damage detection from changes in curvature mode shapes", *J. Sound Vib.*, **145**(2), 321-332.
- Pandey, A.K. and Biswas, M. (1994), "Damage detection in structures using changes in flexibility", *J. Sound Vib.*, **169**(1), 3-17.
- Ryan, K.L. and Chopra, A.K. (2002), "Approximate analysis methods for asymmetric plan base-isolated buildings", *Earthq. Eng. Struct. D.*, **31**(1), 33-54.
- Tena Colunga, A. and Gómez Soberón, L. (2002), "Torsional response of base-isolated structures due to asymmetries in the superstructure", *Eng. Struct.*, **24**(12), 1587-1599.
- Tena Colunga, A. and Zambrana Rojas, C. (2006), "Dynamic torsional amplifications of base-isolated structures with an eccentric isolation system", *Eng. Struct.*, **28**(1), 72-83.
- Tena Colunga, A. and Escamilla Cruz, J.L. (2007), "Torsional amplifications in asymmetric base-isolated structures", *Eng. Struct.*, **29**(2), 237-247.
- Ueng, J.M., Lin, C.C. and Lin, P.L. (2000), "System identification of torsionally-coupled buildings", *Comput. Struct.*, **74**(6), 667-686.
- Ventura, C.E., Liam Finn, W.D., Lord, J.F. and Fujita, N. (2003), "Dynamic characteristics of a base isolated building from ambient vibration measurements and low level earthquake shaking", *Soil Dynam. Earthq. Eng.*, **23**(4), 313-322.
- Wang, J.F., Lin, C.C. and Yen, S.M. (2007), "A story damage index of seismically-excited buildings based on modal frequency and mode shape", *Eng. Struct.*, **29**(9), 2143-2157.
- Yoshimoto, R., Mita, A. and Okada, K. (2005), "Damage detection of base-isolated buildings using multi-input multi-output subspace identification", *Earthq. Eng. Struct. D.*, **34**(3), 307-324.

Appendix

With Eqs. (2.4b) and (2.4c), Eq. (2.5) can be rewritten in detail as

$$\left[\begin{array}{ccc} k_{b_x} & 0 & -k_{b_x} e_y \\ 0 & k_{b_y} & k_{b_y} e_x \\ -k_{b_x} e_y & k_{b_y} e_x & k_{b_x} e_y^2 + k_{b_y} e_x^2 + k_{b_\theta} \end{array} \right] - \omega_j^2 \left[\begin{array}{ccc} m_p & 0 & 0 \\ 0 & m_p & 0 \\ 0 & 0 & J_p \end{array} \right] \begin{Bmatrix} \phi_{x_j} \\ \phi_{y_j} \\ \phi_{\theta_j} \end{Bmatrix} = \begin{Bmatrix} 0 \\ 0 \\ 0 \end{Bmatrix} \quad (\text{A.1})$$

and then

$$\left[\begin{array}{ccc} k_{b_x} - \omega_j^2 m_p & 0 & -k_{b_x} e_y \\ 0 & k_{b_y} - \omega_j^2 m_p & k_{b_y} e_x \\ -k_{b_x} e_y & k_{b_y} e_x & k_{b_x} e_y^2 + k_{b_y} e_x^2 + k_{b_\theta} - \omega_j^2 J_p \end{array} \right] \begin{Bmatrix} \phi_{x_j} \\ \phi_{y_j} \\ \phi_{\theta_j} \end{Bmatrix} = \begin{Bmatrix} 0 \\ 0 \\ 0 \end{Bmatrix} \quad (\text{A.2})$$

Expanding the matrix multiplication in Eq. (A.2) and extracting the first two rows acquire the following system equations

$$(k_{b_x} - \omega_j^2 m_p) \phi_{x_j} - k_{b_x} e_y \phi_{\theta_j} = 0 \quad (\text{A.3})$$

$$(k_{b_y} - \omega_j^2 m_p) \phi_{y_j} - k_{b_y} e_x \phi_{\theta_j} = 0 \quad (\text{A.4})$$

From Eqs. (A.3) and (A.4), k_{b_x} and k_{b_y} can be analytically drawn as

$$k_{b_x} = \omega_j^2 \frac{m_p \phi_{x_j}}{\phi_{x_j} - e_y \phi_{\theta_j}}, \quad k_{b_y} = \omega_j^2 \frac{m_p \phi_{y_j}}{\phi_{y_j} + e_x \phi_{\theta_j}} \quad (\text{A.5, A.6})$$

Dividing numerator and denominator of Eq. (A.5) by ϕ_{x_j} and those of Eq. (A.6) by ϕ_{y_j} , and defining $r_{\phi_x, j} = \phi_{\theta_j} / \phi_{x_j}$ and $r_{\phi_y, j} = \phi_{\theta_j} / \phi_{y_j}$, Eqs. (2.6) and (2.7) are carried out.

Let j_1 and j_2 be two different vibration modes. Thus, from Eqs.(2.6) and (2.7), it can be written that

$$k_{b_y} = \omega_{j_1}^2 \frac{m_p}{1 + e_x r_{\phi_y, j_1}} = \omega_{j_2}^2 \frac{m_p}{1 + e_x r_{\phi_y, j_2}} \quad (\text{A.7})$$

and

$$k_{b_x} = \omega_{j_1}^2 \frac{m_p}{1 - e_y r_{\phi_x, j_1}} = \omega_{j_2}^2 \frac{m_p}{1 - e_y r_{\phi_x, j_2}} \quad (\text{A8})$$

From the latter two terms of Eq. (A.7) and Eq. (A8.), respectively, Eqs. (2.8a) and (2.8b) can be obtained.